



## OPEN ACCESS

## EDITED BY

Yue Li,  
Hefei Institutes of Physical Science  
(CAS), China

## REVIEWED BY

Samir Kumar,  
Korea University, South Korea  
Guangqiang Liu,  
Qufu Normal University, China

## \*CORRESPONDENCE

Xiao Zhang,  
✉ changshui@hotmail.com  
Liang Wang,  
✉ healthscience@foxmail.com

## SPECIALTY SECTION

This article was submitted to Colloidal  
Materials and Interfaces,  
a section of the journal  
Frontiers in Materials

RECEIVED 19 September 2022

ACCEPTED 30 November 2022

PUBLISHED 25 January 2023

## CITATION

Usman M, Ishafaq MU, Muhammad Z,  
Ali W, Dastgeer G, Zhang X and Wang L  
(2023), Evaporation-induced self-  
assembly of gold nanorods on a  
hydrophobic substrate for surface  
enhanced Raman  
spectroscopy applications.  
*Front. Mater.* 9:1048011.  
doi: 10.3389/fmats.2022.1048011

## COPYRIGHT

© 2023 Usman, Ishafaq, Muhammad,  
Ali, Dastgeer, Zhang and Wang. This is an  
open-access article distributed under  
the terms of the [Creative Commons  
Attribution License \(CC BY\)](https://creativecommons.org/licenses/by/4.0/). The use,  
distribution or reproduction in other  
forums is permitted, provided the  
original author(s) and the copyright  
owner(s) are credited and that the  
original publication in this journal is  
cited, in accordance with accepted  
academic practice. No use, distribution  
or reproduction is permitted which does  
not comply with these terms.

# Evaporation-induced self-assembly of gold nanorods on a hydrophobic substrate for surface enhanced Raman spectroscopy applications

Muhammad Usman<sup>1</sup>, M. U. U. Ishafaq<sup>2</sup>, Zahir Muhammad<sup>3</sup>,  
Wajid Ali<sup>4</sup>, Ghulam Dastgeer<sup>5</sup>, Xiao Zhang<sup>1\*</sup> and Liang Wang<sup>1,6\*</sup>

<sup>1</sup>Department of Bioinformatics, School of Medical Informatics and Engineering, Xuzhou Medical University, Xuzhou, China, <sup>2</sup>Hefei National Laboratory for Physical Sciences at Microscale and Department of Physics, University of Science and Technology of China, Hefei, Anhui, China, <sup>3</sup>Hefei Innovation Research Institute, School of Microelectronics, Beihang University, Hefei, China, <sup>4</sup>Key Laboratory for Micro-Nano Physics and Technology of Hunan Province, College of Materials Science and Engineering, Hunan University, Changsha, Hunan, China, <sup>5</sup>Department of Physics and Astronomy and Graphene Research Institute, Sejong University, Seoul, South Korea, <sup>6</sup>Laboratory Medicine, Guangdong Provincial People's Hospital, Guangdong Academy of Medical Sciences, Guangzhou, China

The controllable assembly of plasmonic nanoparticles has developed as one of the most significant approaches for surface enhanced Raman spectroscopy (SERS) applications. This study developed a simple approach to improve a large-scale ordered assembly of gold nanorods (GNRs) by controlling the droplet evaporation mode on hydrophobic substrates. The hydrophobic substrate was efficiently produced by spin coating the silicone oil onto the glass slides and annealing them. The analyte molecule rhodamine (R6G) was employed as a surface-enhanced Raman scattering probe to demonstrate the potential effects of the synthesized arrays. This hydrophobic platform enables the concentration and delivery of analyte molecules into the surface enhanced Raman spectroscopy sensitive site while suppressing the coffee ring effect generated by the smooth contraction motion of the base contact radius of the droplet without any pinning. Thus, the limit of detection (LOD) of the R6G analyte was lowered to  $10^{-10}$  M and the homogenous dispersion of surface enhanced Raman spectroscopy hotspots within the self-assembly reproducible surface enhanced Raman spectroscopy signal. This new method enables a broad range of packing patterns and mechanisms by changing the host nanoparticles in the dispersion.

## KEYWORDS

plasmonic nanoparticles, self-assemblies, hydrophobic surface, coffee ring effect, Raman spectroscopy

## 1 Introduction

The self-assembly of nanoparticles is becoming a common and effective approach for fabricating controlled colloidal patterns (Jana, 2004; Ko et al., 2008; Prasad et al., 2008; Grzelczak et al., 2010; Dai et al., 2011). Several methods for fabricating GNRs arrays have been developed to compact complicated particle structures with diverse symmetry and assembly configurations at the nanoscale (Zhu et al., 2011; Quan et al., 2014; Li et al., 2015; Wang et al., 2015; Lu and Tang, 2016; Luo et al., 2017a; Luo et al., 2017b). The assembly of anisotropic colloidal nanoparticles into complicated well-arranged structures has long been a hot topic in nanoscience due to their distinct collective optical and electronic properties and incorporation into nanophotonics (Zhu et al., 2011; Lu and Tang, 2016; Luo et al., 2017a; Quan et al., 2014; Li et al., 2015; Wang et al., 2015; Xia et al., 2003; Cho et al., 2010; Wang et al., 2012; Sun, 2013; Wang et al., 2015; Xu et al., 2015; Neretina et al., 2016; Abeyweera et al., 2017; Kim et al., 2017). The successful incorporation of such nanoparticles into efficient optoelectronic devices needs reproducible, highly organized, and macroscopic uniformity of performance from the structure (Zhu et al., 2011; Li et al., 2016; Lu and Tang, 2016).

The droplet evaporation has been intensively examined among the diverse approaches used to produce complicated structures due along with its functionality, cost-effectiveness, and broad applicability to numerous nanomaterials (Zhang et al., 2014; Vogel et al., 2015). Moreover, the drying droplet commonly leaves a non-uniform solid-ring on the substrate known as a coffee ring (Deegan et al., 1997). The configuration of a solid ring structure is strongly related to droplet-controlled dispersion, which is primarily focused on heat and mass loss during evaporation (Deegan, 2000). The heat loss causes evaporative cooling to sufficiently produce a surface tension slope capable of driving Marangoni flow (Larson, 2014). The evaporation process causes capillary flow outward from the center of the drop, bringing the suspension particles to the edges. The particles are significantly concentrated along the initial drop edge after evaporation, resulting in a non-uniform solid ring (Deegan et al., 2000). Recent research has focused on addressing the coffee-ring effect by controlling important configurations including particle size, particle shape, charges and surfactant concentration, to attain large-area arrays of self-assembled particles (Fan et al., 2004; Bigioni et al., 2006; Byun et al., 2010; Alvarez-Puebla et al., 2011; Singh et al., 2012; Chen et al., 2013; Peng et al., 2013; Ye et al., 2013; Peng et al., 2014; Zhang and Lin, 2014; Apte et al., 2015; Hamon et al., 2015; Li et al., 2016; Lu and Tang, 2016; Luo et al., 2017a; Luo et al., 2017b; Kim et al., 2017). The most effective method for overcoming the “diffusion limit” of analytes in highly diluted aqueous solutions is to use super hydrophobic surfaces, which have the dynamic ability to deliver analytes to SERS-active sites (De Angelis et al., 2011; Gentile et al., 2014). Moreover, the disadvantage of super hydrophobic surfaces for these applications is that air pockets among the surface structures can be spoiled by outward wetting pressure and could lose wetting property by destructive the surface structure (Reyssat et al., 2007).

Recently, slippery surfaces (hydrophobic surfaces) have evolved into a superior substitute to super hydrophobic as a fluid repellent surface with a very small contact angle hysteresis (Bocquet and Lauga, 2011). To our understanding, only few studies has been accompanied on the controlled evaporation method-based SERS technique for analyte detection on cost-effective hydrophilic substrates.

This study proposed a novel method for fabricating self-assembled GNRs. The hydrophobic surface was fabricated in the first step and then controlled the evaporation rate of droplets in the second step. This method was used to reverse the coffee ring effect during droplet evaporation of an aqueous diffusion of GNRs assembly. The droplet evaporation process revealed GNRs formed at the interface between solvent and air, developing domains that improved in size and density as the solvent evaporated under microscope light. The optical properties of the attained superstructures were experimentally determined. Finally, the promising application of GNRs self-assembly arrays for analytical detection using R6G as a model analyte based on SERS was established.

## 2 Material and method

### 2.1 Preparation of GNRs

The study synthesized the GNRs and employed a seed-mediated growth method as described in our previous procedure (Usman et al., 2019). After the seed solution was formed, HAuCl<sub>4</sub> (0.1 ml; 0.025 M) and CTAB (5 ml; 0.2 M) were combined at room temperature. The solution of ice-cold NaBH<sub>4</sub> (0.01 M, 0.6 ml) was promptly introduced. The color of the solution gradually changed from yellow to brownish-yellow. The solution continues to stirring for 20 min. The solution was cooled down to room temperature for 30 min. The growth solution was prepared by adding hexadecyltrimethyl ammonium bromide (CTAB), 5 ml, 0.2 M, and different amounts of 0.05, 0.10, 0.15, 0.20, and 0.25 ml of 0.16 mM AgNO<sub>3</sub> solutions at 30°C, respectively. Then, add 0.2 ml of 0.025 M HAuCl<sub>4</sub> to the solution. Following constant stirring, the ascorbic acid (0.08 M, 70 ml) was added and changed the color from dark-yellow to colorless. Lastly, the seed solution of 12 ml was mixed with the growth solution at 30°C. The color of the mixture slowly changes in 15–30 min. The GNRs were well designed at room temperature after rapid growth.

### 2.2 Silicone oil-based hydrophobic surface preparation

The glass slides were cleaned for 10 min using sonication and plasma cleaning. The silicone oil, with a kinematic viscosity of 370 cSt, was applied to a clean glass slide and spin-coated at 1,000 rpm for 1 min. This method was effective for removing additional lubricating

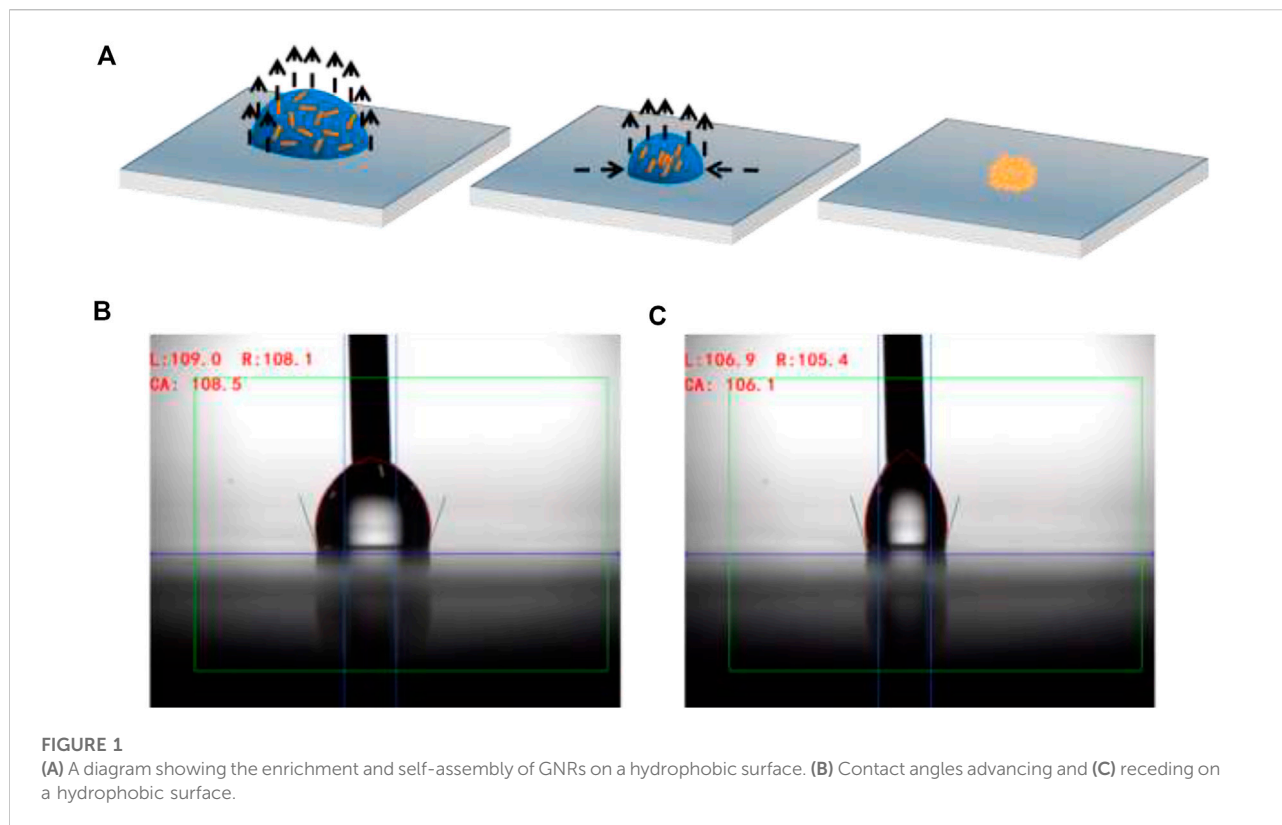


FIGURE 1

(A) A diagram showing the enrichment and self-assembly of GNRs on a hydrophobic surface. (B) Contact angles advancing and (C) receding on a hydrophobic surface.

oil. The silicone oil-coated glass slide was then annealed at 150°C for 120 min. As a result, the surface chemical property was modified to be hydrophobic and a uniform silicone oil coating was formed on the glass slide.

### 2.3 Evaporation-induced assembly of aligned GNRs arrays

The GNRs were centrifuged at 7,000 rpm for 20 min to reduce extra CTAB. A 30- $\mu$ l drop of GNRs was deposited on the hydrophobic substrate. Then the hydrophobic substrate was transferred onto a polystyrene Petri dish plate with dimensions of 94 mm in width and 15 mm in height. After that, add 1 ml of water to the Petri dish to regulate the humidity. The Petri dish was wrapped and put inside an incubator. After the evaporation, the GNRs solution on the hydrophobic substrate contracted into tiny droplets without forming coffee-rings. As a result, the well-arranged assemblies of GNRs were observed on the hydrophobic substrate.

### 2.4 Raman spectroscopy measurements

For the SERS measurements, R6G dye was working as a Raman probe molecule and was diluted to various concentrations. The concentrated molecules and GNRs solution of 30  $\mu$ l was placed on

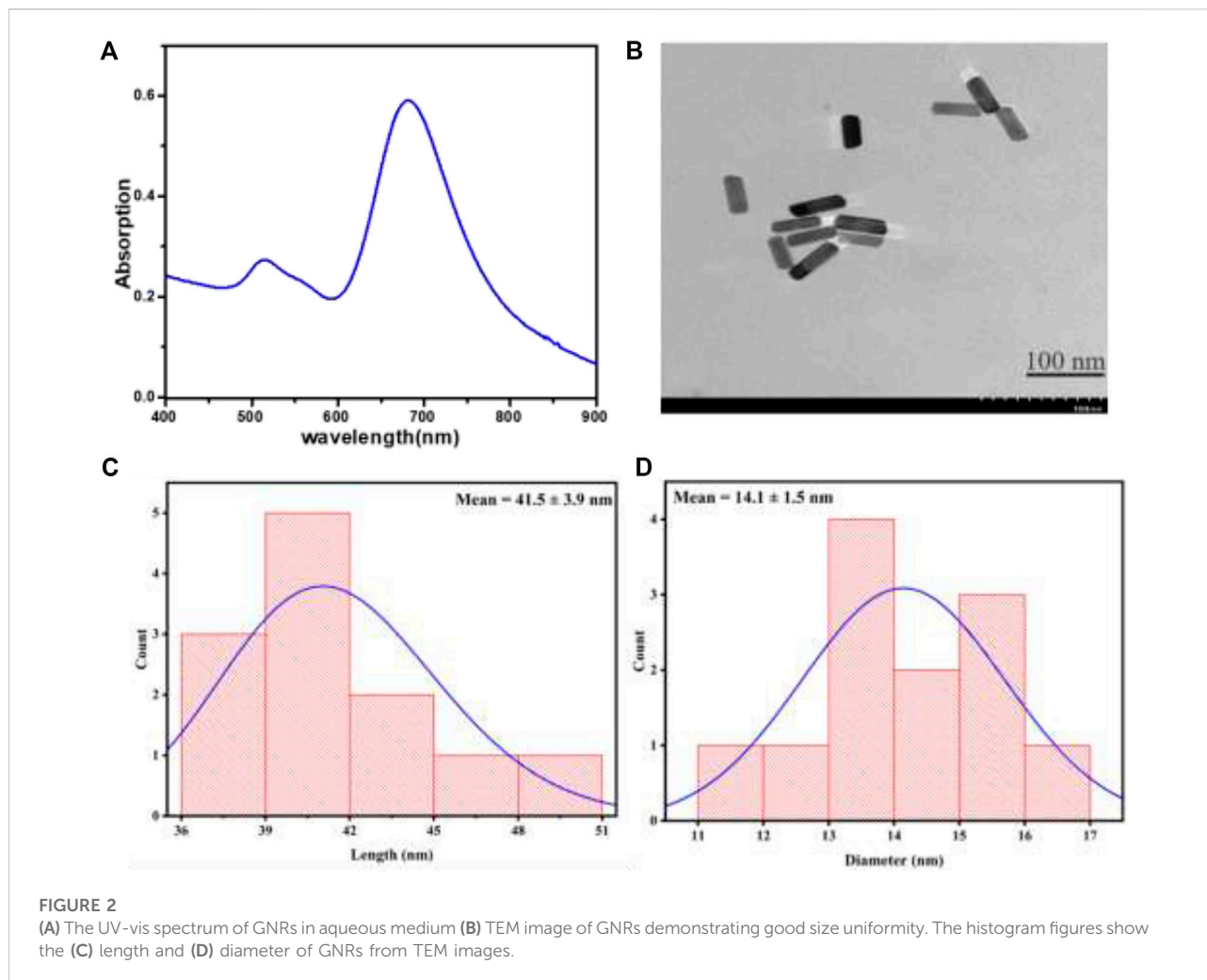
the SERS substrate and evaporated at room temperature. All SERS measurements were carried out using a 633 nm laser excitation and a laser power of about 1.5 mW. A confocal Raman microscope (Renishaw PLC., England, United Kingdom) with a 50-microscope objective and a numerical aperture (NA) of 0.6 was used to detect in-elastically scattered radiation.

### 2.5 FEM simulation

We used the commercial program COMSOL Multiphysics 5.5 for numerical simulation to do electromagnetic analysis. Comsol uses the finite element method (FEM) to solve the following differential form of the Maxwell equation:

$$\nabla \times \frac{1}{\mu_r} (\nabla \times E) - K_0^2 \left( \epsilon_r - \frac{j\sigma}{\omega\epsilon_0} \right) E = 0 \quad (1)$$

where  $\mu_r$  and  $\epsilon_r$  are the medium's relative permittivity and permeability, respectively, and  $K$  is the wave's propagation vector for all mediums in the model,  $\omega$  is the angular frequency, and  $\sigma$  is the medium's conductivity. A 3D frequency-domain model is used to solve the problem in the wave optics module. A perfect matching layer PML is applied at the top and bottom of the model to secure the physical domain from any background fields. Furthermore, periodic boundary conditions

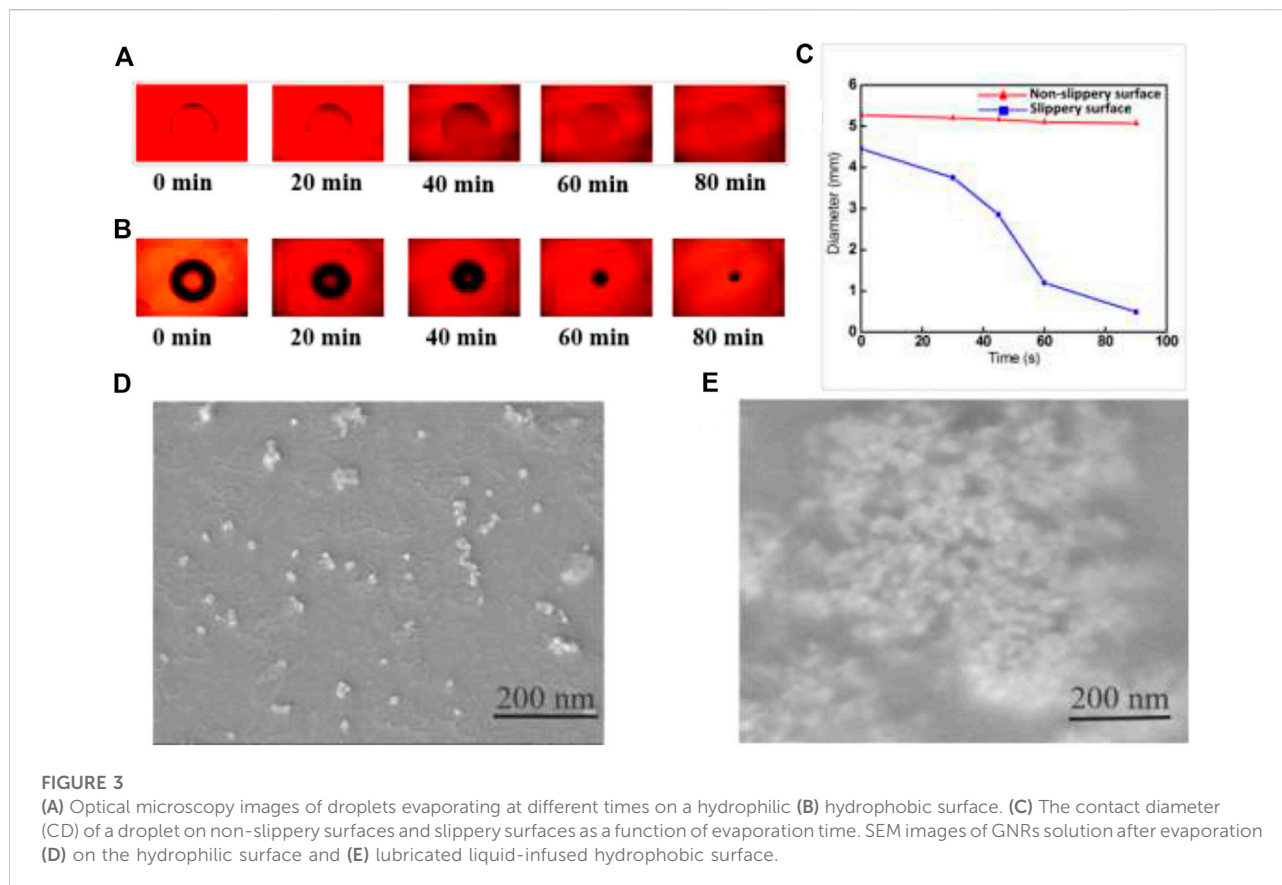


are applied in the  $X$  and  $Y$  directions to simulate light propagation through the hexagonal unit cell of the standing GNRs. Physic controlled fine meshing used for GNRs and physical domain. The whole structure is irradiated vertically with a transverse electric polarized light with an electric field intensity of  $1\text{V/m}$ . The GNRs array in the simulations has a surface-to-surface separation  $p = 7\text{ nm}$ , diameter  $D$  of  $17\text{ nm}$ , and a height of  $30\text{ nm}$ . P. B. Johnson and R. W. Christy experimentally determined values for gold permittivity was utilized for the model. The dielectric constants of the silicone layer and quartz glass were also sourced from the comsol material library.

### 3 Results and discussion

The hydrophobic surface and high humidity environment are critical for GNRs self-assembly and enrichment. A lubricated substrate containing a silicon oil-coated glass slide is a simple

depiction followed by spin coating and annealing. Hence, this would make the substrate hydrophobic because the high surface energy of silicon dioxide changes the surface energy of the glass through covalent bonding of silicone oil molecules with the glass surface. The hydrophobic surface played an important part in the development and self-assembly of GNRs. It is extremely important to keep droplet evaporation in a steady-state assembly process, which is primarily a thermodynamic procedure, in imperative to produce homogeneous self-assembled particle arrays. As a result, the environmental parameters must be carefully monitored, including the temperature and humidity of the substrates during the evaporation process. When the temperature falls below  $25^\circ\text{C}$ , the CTAB surfactant in the droplets crystallizes and precipitates from the solution. This clearly devastates the self-assembly process, resulting in poor quality GNRs arrays. When the temperature rises to  $50^\circ\text{C}$ , however, the convection in the droplet intensifies, causing serious damage in large non-uniform accumulations (Ming et al., 2008). The evaporation

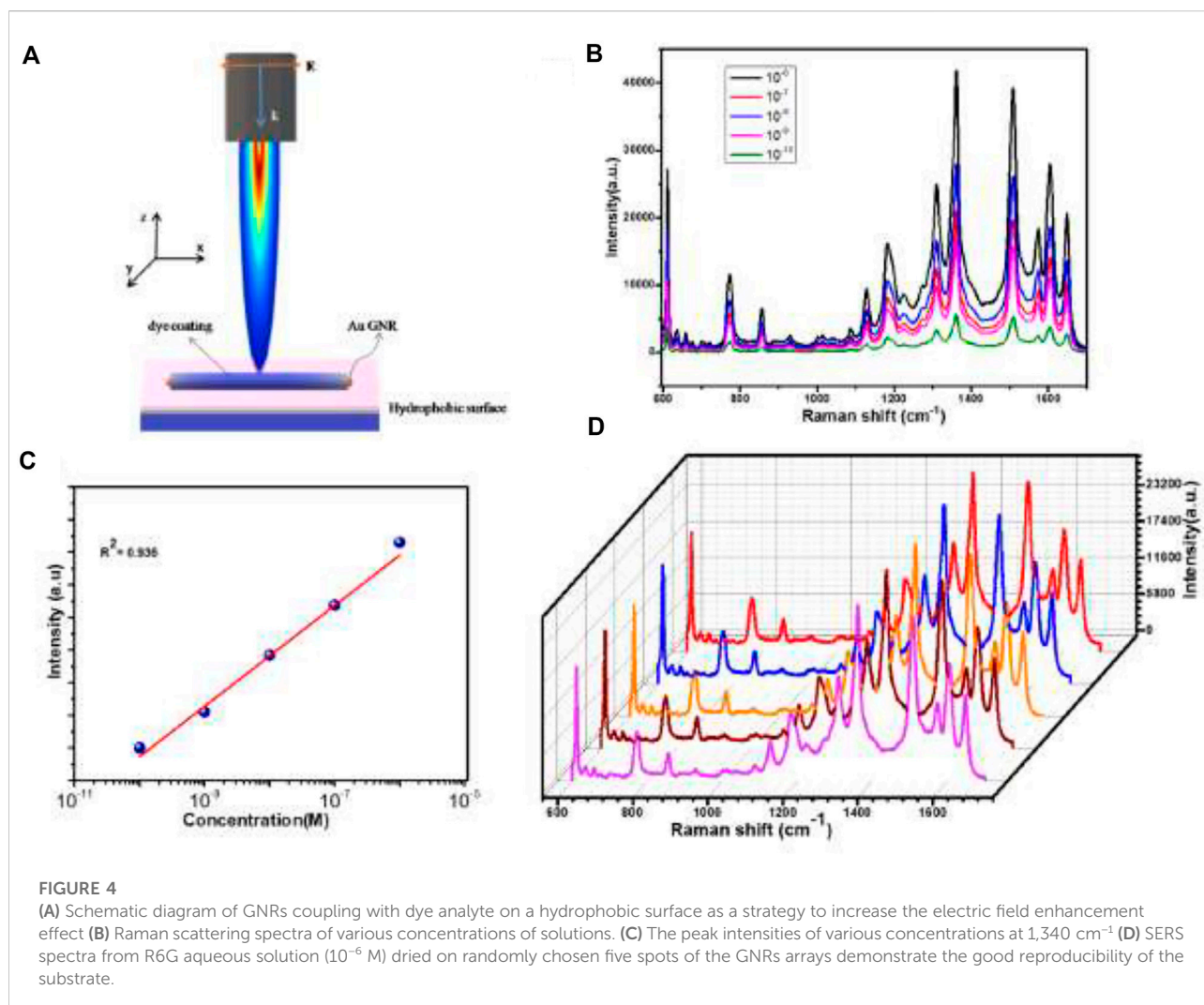


was carried out in a controlled environment with a high humidity level in maintenance. The high humidity environment slowed the evaporation of the GNRs droplets, allowing the solvent to evaporate at the same rate from the contact line to the droplet centers (Zhang and Lin, 2014). The slow evaporation could reduce the convection and inhibit GNRs from following from the center to the contact line, thus preventing the formation of a coffee-ring structure (Hu and Larson, 2006). The solution contracted into smaller droplets owing to the homogeneous evaporation speed and the absence of a pinned edge across the surface of the droplets. Figure 1A depicts a schematic demonstration of the fabrication method of the hydrophobic platform.

After optimizing the conditions, we investigated the effects of substrate hydrophobicity and repellency by contact angle ( $\theta$ ) and contact angle hysteresis (CAH) ( $\Delta\theta = \theta_a - \theta_r$ ), the difference between the advancing ( $\theta_a$ ) and receding contact angle ( $\theta_r$ ) measured by optical Goniometer (OCA35, Data Physics Germany). Figure 1B showed substrates with GNRs contact angles of  $108.5^\circ$ , indicating the value of the fabricated hydrophobic surface was tremendous. Contact angle hysteresis ( $\Delta\theta$ ) is associated with the pinning of the contact line and characterizes the droplet evaporation process. In the case of contact line pinning, the contact angle decreases as the

droplet volume decreases and the contact line starts to withdraw. Contact-angle hysteresis during droplet evaporation reflects the contact line receding in this way. In our case,  $\Delta\theta$  on a hydrophobic surface was only  $2.4^\circ$ , as shown in Figure 1C, which demonstrated that the fabricated hydrophobic surface was of high quality. The small contact angle hysteresis of the dispersion of GNRs on the hydrophobic surface helps to reverse the coffee-ring effect. It can be established that Marangoni flow and contact line receding can efficiently control the final configuration of GNRs on the substrate. This process avoids the coffee-ring effect that occurs during nanoparticle evaporation, resulting in uniform deposition and adjacent packing of GNRs.

This study used an evaporation-induced self-assembly approach to obtain GNRs from a liquid drop containing GNRs. The UV-vis absorption spectrum of GNRs dispersed in water is shown in Figure 2A. The transverse and longitudinal modes were assigned to the surface plasmon resonance peaks that were obtained at wavelengths of 510 and 670 nm, respectively. The previous research has shown that the maximum SERS intensity was achieved when the laser excitation wavelength was slightly shorter than LSPR, so the laser excitation wavelength was in resonance with the substrate of the surface plasmon (Hossain et al., 2009; Kumar et al., 2020). Figure 2B depicts a transmission electron microscopy (TEM)



representation of GNRs. The distributions of GNRs particle sizes measured in TEM images were plotted in (Figures 2C, D). The length of  $41.5 \pm 3.9\text{ nm}$  and the width of  $14.1 \pm 1.5\text{ nm}$  of the GNRs were obtained from the histogram diagram, and an aspect ratio of about 3. According to this, GNRs had uniform morphology and a narrow size distribution.

We investigated the effects of hydrophobicity on the development of GNRs arrays after optimizing the evaporation conditions, such as temperature at  $30^{\circ}\text{C}$  and humidity at 96%. The GNRs evaporated on the hydrophobic surface in a controlled environment, producing a highly concentrated pattern and repellency. The  $20\text{ }\mu\text{l}$  GNRs were measured using an optical microscope at various times on hydrophilic and hydrophobic substrates (see Figure 3).

The droplet of the initial contact diameter ( $d$ ) on the non-slippery surface (hydrophilic surface) was large ( $d = 4.47\text{ mm}$ ). The contact diameter did not change significantly over the evaporation time due to the hydrophilic nature of the

particles and the droplet spread over a large spot with a diameter of  $4.27\text{ mm}$  after completely solvent drying (after 55 min), as shown in Figure 3A. On the other hand, the contact diameter of the droplet on the hydrophobic surface was reduced to  $0.193\text{ mm}$  from its initial diameter of  $3.154\text{ mm}$  after complete drying of the solvent, which was smaller than that of a droplet of the same volume on the hydrophilic surface due to surface hydrophobicity as revealed in Figure 3B. The contact diameter of hydrophilic and hydrophobic surfaces varied with the evaporation time, as shown in Figure 3C. The hydrophobic surface reduced contact area by approximately 98.78% when compared to the hydrophilic surface.

The scanning electron microscopy (SEM) images suggest an exciting effect of the enrichment and the concentration of GNRs particles on hydrophilic and hydrophobic surfaces after evaporation. In Figure 3D, the GNRs particles showed a scattered pattern after complete evaporation on a hydrophilic

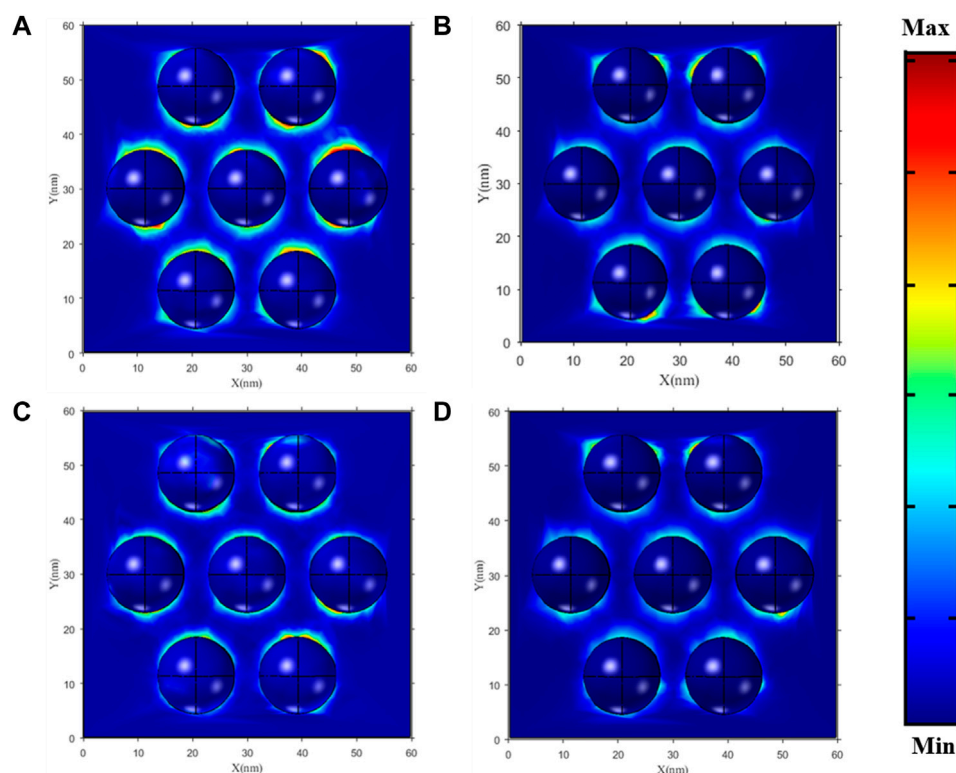


**FIGURE 5**

The enhancement of the electromagnetic field in GNRs with hydrophobic and hydrophilic substrates with 7-nm gaps (A,C) and (B,D), respectively.

surface, with the maximum value at the droplet edge, as described by the “coffee ring effect.” This effect is commonly observed at pinning sites on surfaces. As a result, GNRs particles show an extensive configuration over a large area. However, the GNRs solution produced interesting results on the hydrophobic surface. The easy contraction of the droplet without pinning suppressed the coffee ring effect to enrich all the GNRs particles into a very small spot on the hydrophobic surface. The effective compact self-assembly of GNRs *via* droplet evaporation on the hydrophobic surface is shown in Figure 3E.

Furthermore, the condition for a high contact angle and low CAH is critical for improving SERS performance. In former studies has demonstrated that densely compacted metallic nanoparticles have significant SERS enhancement factors (Diebold et al., 2009; Huang et al., 2015). The formation of the hot spots between neighboring particles significantly increases SERS enhancement.

In this study, the fabricated substrate was covered by a closely packed GNRs array, which produced a significant field enhancement effect. The schematically Figure 4A illustrates the encapsulated GNRs on a hydrophobic surface. Here a rounded ends cylindrical GNRs (with orange color) coated

with dye (blue color), shined by TE polarized light. The electric field is parallel to the plane of the hydrophobic surface with normal K-propagation vector. The densely-packed GNRs arrays and their uniform structure were able to produce a SERS signal for molecular detection at concentrations as low as  $10^{-10}$  M. SERS measurements on the GNRs arrays were carried out using a Raman spectrometer with a 633 nm excitation. The target molecule was R6G solution, a common dye used in biological research. Figure 4B shows the SERS spectra of R6G at various concentrations ranging from  $10^{-6}$  to  $10^{-10}$  M. The Raman spectra of R6G were attributed to C-C-C ring in plane, out-of-plane being, and C-H in-plane bending vibrations in the sharp peaks at 611 and 776  $\text{cm}^{-1}$ , respectively. It also had Raman shift peaks at 1,180, 1,360, 1,509, and 1,650  $\text{cm}^{-1}$ , which were ascribed to symmetric modes of C-C stretching vibrations in plane. These R6G Raman peaks are consistent with those previously reported (Lu et al., 2005; Jensen and Schatz, 2006). The Raman spectra clearly showed the characteristic Raman peaks of R6G even when the concentration was as low as  $10^{-10}$  M. The SERS substrates for the GNRs arrays had excellent reusability, enabling multiple detections after plasma etching to clean the previous substrate. The Raman signal

decreased gradually with the decreasing the concentration of R6G. The previous results were also confirmed in the study of Wei et al. (2018) using R6G detection at a concentration was as low as  $10^{-10}$  M. We obtained the calibration curves with this result analyzed as shown in Figure 4C. Notably, it had a relatively good linear correlation relationship (correlation coefficient,  $R^2 = 0.9928$ ) between the SERS signal ratio and R6G concentration. The suggested approach might, therefore, prove helpful in the quantitative analysis.

In order to study the uniformity and ensure a homogeneous distribution,  $10^{-6}$  M of the analyte R6G aqueous solution was dispersed on the surface of the hydrophobic surface. After that, we observed five random spots on the substrate with the same exciting line and integration time (Figure 4D). The relative signal deviation of R6G was about 10% on the GNRs arrays, revealing the overall reliability and uniformity of such a substrate for SERS detection. The excellent performance of the GNRs arrays could be attributed to a number of factors. For example, the GNRs were arranged in a regular pattern. In periodic structures, photon density redistribution was common, causing an increase in the density of optical modes and an improvement in the Raman scattering of the detected molecules (Gaponenko, 2002).

To effectively understand the physical mechanism underlying the detected SERS response, the electric field intensity enhancement of the GNRs array was investigated employing Comsol multiphysics simulation (see Figure 5), on hydrophobic and hydrophilic substrates, under 540 and 670 nm laser light. The GNRs arrays are assembled with a gap of 7 nm. The GNRs revealed the enhancement of electromagnetic fields in the case of the hydrophobic surface. Figure 5A indicates that at 540 nm of laser excitation, the field is a maximally localized electromagnetic field within the GNRs array in the hydrophobic substrate compared to the hydrophilic substrate in Figure 5B. Similarly, Figure 5C exhibits a similar excellent local field enhancement effect on a hydrophobic substrate as compared to the hydrophilic substrate using 670 nm laser excitation. Hence, when compared with the disordered substrate, the resonance of the local electromagnetic field around the GNRs arrays is relatively strong, and the dense “hot spots” can improve the SERS activity of the substrate. These results further confirm and demonstrate that the hydrophobic substrate can be used to enhance and detect the SERS signals, which is almost consistent with our experimental results.

## 4 Conclusion

In summary, we used the controlled evaporation process to fabricate large-area ordered self-assembly arrays of GNRs on the hydrophobic surface. The droplet contracts effectively because of the lack of pinning sites and hydrophobicity of the substrate, which prevent the coffee-ring effect and offer a smooth surface. Therefore, this process effectively delivers the molecules inside the droplet to a

concentrated hot spot. The resulting arrays had constant structural and efficient homogeneity on a macroscopic scale. We also established that the fabricated GNRs arrays produced a SERS signal for detecting R6G at a concentration of  $10^{-10}$  M. The exceptional results in SERS detection reproducibility are due to the uniformity in large areas. The structure of the GNRs relied solely on the hydrophobicity of substrates in an evaporating environment. The limitation of hydrophobic surfaces is also observed when there are many liquid drops sliding on them, which slowly removes the lubricating oil. In this case, the hydrophobic performance is degraded, but it can be rapidly recovered by coating the silicone oil on the surface again. As a result, this technology could be easily applied to different nanoparticle systems to produce ordered nanoscale arrays for the integration of microscopic devices.

## Data availability statement

The original contributions presented in the study are included in the article/Supplementary Material, further inquiries can be directed to the corresponding authors.

## Author contributions

MU conceived the core ideas and designed the outlines of the manuscript. MI and ZM contributed to the project administration. WA carried out the theoretical simulation analysis of literature. All authors made significant contributions to write and revise the manuscript. XZ and LW set-up the platforms, provided resources, and secured funding for the study. All authors read and approved the submitted version of the manuscript.

## Funding

This work was supported in part by National Natural Science Foundation of China (31900022, 32171281), Young Science and Technology Innovation Team of Xuzhou Medical University (TD202001), and Jiangsu Qinglan Project (2020).

## Acknowledgments

We acknowledge the assistance from the scanning electron microscopy analysis.

## Conflict of interest

The authors declare that the research was conducted in the absence of any commercial or financial relationships that could be construed as a potential conflict of interest.

## Publisher's note

All claims expressed in this article are solely those of the authors and do not necessarily represent those of their affiliated

organizations, or those of the publisher, the editors and the reviewers. Any product that may be evaluated in this article, or claim that may be made by its manufacturer, is not guaranteed or endorsed by the publisher.

## References

- Abeyweera, S. C., Rasamani, K. D., and Sun, Y. (2017). Ternary silver halide nanocrystals. *Acc. Chem. Res.* 50, 1754–1761. doi:10.1021/acs.accounts.7b00194
- Alvarez-Puebla, R. A., Agarwal, A., Manna, P., Khanal, B. P., Aldeanueva-Potel, P., Carbó-Argibay, E., et al. (2011). Gold nanorods 3D-supercrystals as surface enhanced Raman scattering spectroscopy substrates for the rapid detection of scrambled prions. *Proc. Natl. Acad. Sci.* 108, 8157–8161. doi:10.1073/pnas.1016530108
- Apte, A., Bhaskar, P., Das, R., Chaturvedi, S., Poddar, P., and Kulkarni, S. (2015). Self-assembled vertically aligned gold nanorod superlattices for ultra-high sensitive detection of molecules. *Nano Res.* 8, 907–919. doi:10.1007/s12274-014-0572-2
- Bigioni, T. P., Lin, X. M., Nguyen, T. T., Corwin, E. I., Witten, T. A., and Jaeger, H. M. (2006). Kinetically driven self-assembly of highly ordered nanoparticle monolayers. *Nat. Mat.* 5, 265–270. doi:10.1038/nmat1611
- Bocquet, L., and Lauga, E. (2011). A smooth future? *Nat. Mat.* 10, 334–337. doi:10.1038/nmat2994
- Byun, M., Bowden, N. B., and Lin, Z. (2010). Hierarchically organized structures engineered from controlled evaporative self-assembly. *Nano Lett.* 10, 3111–3117. doi:10.1021/nl1018035
- Chen, H., Shao, L., Li, Q., and Wang, J. (2013). Gold nanorods and their plasmonic properties. *Chem. Soc. Rev.* 42, 2679–2724. doi:10.1039/c2cs35367a
- Cho, E. C., Camargo, P. H., and Xia, Y. (2010). Synthesis and characterization of noble-metal nanostructures containing gold nanorods in the center. *Adv. Mat.* 22, 744–748. doi:10.1002/adma.200903097
- Dai, Q., Rettner, C. T., Davis, B., Cheng, J., and Nelson, A. (2011). Topographically directed self-assembly of gold nanoparticles. *J. Mat. Chem.* 21, 16863–16865. doi:10.1039/c1jm11683e
- De Angelis, F., Gentile, F., Mecerini, F., Das, G., Moretti, M., Candeloro, P., et al. (2011). Breaking the diffusion limit with super-hydrophobic delivery of molecules to plasmonic nanofocusing SERS structures. *Nat. Photonics* 5, 682–687. doi:10.1038/nphoton.2011.222
- Deegan, R. D., Bakajin, O., Dupont, T. F., Huber, G., Nagel, S. R., and Witten, T. A. (1997). Capillary flow as the cause of ring stains from dried liquid drops. *Nature* 389, 827–829. doi:10.1038/39827
- Deegan, R. D., Bakajin, O., Dupont, T. F., Huber, G., Nagel, S. R., and Witten, T. A. (2000). Contact line deposits in an evaporating drop. *Phys. Rev. E* 62, 756–765. doi:10.1103/physreve.62.756
- Deegan, R. D. (2000). Pattern formation in drying drops. *Phys. Rev. E* 61, 475–485. doi:10.1103/physreve.61.475
- Diebold, E. D., Mack, N. H., Doorn, S. K., and Mazur, E. (2009). Femtosecond laser-nanostructured substrates for surface-enhanced Raman scattering. *Langmuir* 25, 1790–1794. doi:10.1021/la803357q
- Fan, H., Yang, K., Boye, D. M., Sigmon, T., Malloy, K. J., Xu, H., et al. (2004). Self-assembly of ordered, robust, three-dimensional gold nanocrystal/silica arrays. *Science* 304, 567–571. doi:10.1126/science.1095140
- Gaponenko, S. V. (2002). Effects of photon density of states on Raman scattering in mesoscopic structures. *Phys. Rev. B* 65, 140303. doi:10.1103/physrevb.65.140303
- Gentile, F., Coluccio, M. L., Zaccaria, R. P., Francardi, M., Cojoc, G., Perozziello, G., et al. (2014). Selective on site separation and detection of molecules in diluted solutions with super-hydrophobic clusters of plasmonic nanoparticles. *Nanoscale* 6, 8208–8225. doi:10.1039/c4nr00796d
- Grzelczak, M., Vermant, J., Furst, E. M., and Liz-Marzán, L. M. (2010). Directed self-assembly of nanoparticles. *ACS Nano* 4, 3591–3605. doi:10.1021/nn100869j
- Hamon, C., Novikov, S. M., Scarabelli, L., Solís, D. M., Altantzis, T., Bals, S., et al. (2015). Collective plasmonic properties in few-layer gold nanorod supercrystals. *ACS Photonics* 2, 1482–1488. doi:10.1021/acsphotonics.5b00369
- Hossain, M. K., Kitahama, Y., Huang, G. G., Han, X., and Ozaki, Y. (2009). Surface-enhanced Raman scattering: Realization of localized surface plasmon resonance using unique substrates and methods. *Anal. Bioanal. Chem.* 394, 1747–1760. doi:10.1007/s00216-009-2762-4
- Hu, H., and Larson, R. G. (2006). Marangoni effect reverses coffee-ring depositions. *J. Phys. Chem. B* 110, 7090–7094. doi:10.1021/jp0609232
- Huang, L., Mühlenbernd, H., Li, X., Song, X., Bai, B., Wang, Y., et al. (2015). Broadband hybrid holographic multiplexing with geometric metasurfaces. *Adv. Mat.* 27, 6444–6449. doi:10.1002/adma.201502541
- Jana, N. R. (2004). Shape effect in nanoparticle self-assembly. *Angew. Chem. Int. Ed.* 43, 1536–1540. doi:10.1002/anie.200352260
- Jensen, L., and Schatz, G. C. (2006). Resonance Raman scattering of rhodamine 6G as calculated using time-dependent density functional theory. *J. Phys. Chem. A* 110, 5973–5977. doi:10.1021/jp0610867
- Kim, J., Song, X., Ji, F., Luo, B., Ice, N. F., Liu, Q., et al. (2017). Polymorphic assembly from beveled gold triangular nanoprisms. *Nano Lett.* 17, 3270–3275. doi:10.1021/acs.nanolett.7b00958
- Ko, H., Singamaneni, S., and Tsukruk, V. V. (2008). Nanostructured surfaces and assemblies as SERS media. *Small* 4, 1576–1599. doi:10.1002/sml.200800337
- Kumar, S., Tokunaga, K., Namura, K., Fukuoka, T., and Suzuki, M. (2020). Experimental evidence of a twofold electromagnetic enhancement mechanism of surface-enhanced Raman scattering. *J. Phys. Chem. C* 124, 21215–21222. doi:10.1021/acs.jpcc.0c07930
- Larson, R. G. (2014). Transport and deposition patterns in drying sessile droplets. *AIChE J.* 60, 1538–1571. doi:10.1002/aic.14338
- Li, P., Li, Y., Zhou, Z. K., Tang, S., Yu, X. F., Xiao, S., et al. (2016). Evaporative self-assembly of gold nanorods into macroscopic 3D plasmonic superlattice arrays. *Adv. Mat.* 28, 2511–2517. doi:10.1002/adma.201505617
- Li, R., Bian, K., Wang, Y., Xu, H., Hollingsworth, J. A., Hanrath, T., et al. (2015). An obtuse rhombohedral superlattice assembled by Pt nanocubes. *Nano Lett.* 15, 6254–6260. doi:10.1021/acs.nanolett.5b02879
- Lu, C., and Tang, Z. (2016). Advanced inorganic nanoarchitectures from oriented self-assembly. *Adv. Mat.* 28, 1096–1108. doi:10.1002/adma.201502869
- Lu, Y., Liu, G. L., and Lee, L. P. (2005). High-density silver nanoparticle film with temperature-controllable interparticle spacing for a tunable surface enhanced Raman scattering substrate. *Nano Lett.* 5, 5–9. doi:10.1021/nl048965u
- Luo, B., Smith, J. W., Ou, Z., and Chen, Q. (2017). Quantifying the self-assembly behavior of anisotropic nanoparticles using liquid-phase transmission electron microscopy. *Acc. Chem. Res.* 50, 1125–1133. doi:10.1021/acs.accounts.7b00048
- Luo, B., Smith, J. W., Wu, Z., Kim, J., Ou, Z., and Chen, Q. (2017). Polymerization-like co-assembly of silver nanoplates and patchy spheres. *ACS Nano* 11, 7626–7633. doi:10.1021/acsnano.7b02059
- Ming, T., Kou, X., Chen, H., Wang, T., Tam, H. L., Cheah, K. W., et al. (2008). Ordered gold nanostructure assemblies formed by droplet evaporation. *Angew. Chem. Int. Ed.* 47, 9831–9836. doi:10.1002/ange.200803642
- Neretina, S., Hughes, R. A., Gilroy, K. D., and Hajfathalian, M. (2016). Noble metal nanostructure synthesis at the liquid–substrate interface: New structures, new insights, and new possibilities. *Acc. Chem. Res.* 49, 2243–2250. doi:10.1021/acs.accounts.6b00393
- Peng, B., Li, G., Li, D., Dodson, S., Zhang, Q., Zhang, J., et al. (2013). Vertically aligned gold nanorod monolayer on arbitrary substrates: Self-assembly and femtomolar detection of food contaminants. *ACS Nano* 7, 5993–6000. doi:10.1021/nn401685p
- Peng, B., Li, Z., Mutlugun, E., Martinez, P. L. H., Li, D., Zhang, Q., et al. (2014). Quantum dots on vertically aligned gold nanorod monolayer: Plasmon enhanced fluorescence. *Nanoscale* 6, 5592–5598. doi:10.1039/c3nr06341k
- Prasad, B. L. V., Sorensen, C. M., and Klabunde, K. J. (2008). Gold nanoparticle superlattices. *Chem. Soc. Rev.* 37, 1871–1883. doi:10.1039/b712175j
- Quan, Z., Xu, H., Wang, C., Wen, X., Wang, Y., Zhu, J., et al. (2014). Solvent-mediated self-assembly of nanocube superlattices. *J. Am. Chem. Soc.* 136, 1352–1359. doi:10.1021/ja408250q
- Reyssat, M., Yeomans, J. M., and Quéré, D. (2007). Impalement of fakir drops. *Europhys. Lett.* 81, 26006. doi:10.1209/0295-5075/81/26006

Singh, A., Gunning, R. D., Ahmed, S., Barrett, C. A., English, N. J., Garate, J. A., et al. (2012). Controlled semiconductor nanorod assembly from solution: Influence of concentration, charge and solvent nature. *J. Mat. Chem.* 22, 1562–1569. doi:10.1039/c1jm14382d

Sun, Y. (2013). Controlled synthesis of colloidal silver nanoparticles in organic solutions: Empirical rules for nucleation engineering. *Chem. Soc. Rev.* 42, 2497–2511. doi:10.1039/c2cs35289c

Usman, M., Guo, X., Wu, Q., Barman, J., Su, S., Huang, B., et al. (2019). Facile silicone oil-coated hydrophobic surface for surface enhanced Raman spectroscopy of antibiotics. *RSC Adv.* 9, 14109–14115. doi:10.1039/c9ra00817a

Vogel, N., Retsch, M., Fustin, C. A., Del Campo, A., and Jonas, U. (2015). Advances in colloidal assembly: The design of structure and hierarchy in two and three dimensions. *Chem. Rev.* 115, 6265–6311. doi:10.1021/cr400081d

Wang, C., Siu, C., Zhang, J., and Fang, J. (2015). Understanding the forces acting in self-assembly and the implications for constructing three-dimensional (3D) supercrystals. *Nano Res.* 8, 2445–2466. doi:10.1007/s12274-015-0767-1

Wang, T., Zhuang, J., Lynch, J., Chen, O., Wang, Z., Wang, X., et al. (2012). Self-assembled colloidal superparticles from nanorods. *Science* 338, 358–363. doi:10.1126/science.1224221

Wei, W., Wang, Y., Ji, J., Zuo, S., Li, W., Bai, F., et al. (2018). Fabrication of large-area arrays of vertically aligned gold nanorods. *Nano Lett.* 18, 4467–4472. doi:10.1021/acs.nanolett.8b01584

Xia, Y., Yang, P., Sun, Y., Wu, Y., Mayers, B., Gates, B., et al. (2003). One-dimensional nanostructures: Synthesis, characterization, and applications. *Adv. Mat.* 15, 353–389. doi:10.1002/adma.200390087

Xu, H., Xu, Y., Pang, X., He, Y., Jung, J., Xia, H., et al. (2015). A general route to nanocrystal kebabs periodically assembled on stretched flexible polymer shish. *Sci. Adv.* 1, 1500025. doi:10.1126/sciadv.1500025

Ye, X., Millan, J. A., Engel, M., Chen, J., Diroll, B. T., Glotzer, S. C., et al. (2013). Shape alloys of nanorods and nanospheres from self-assembly. *Nano Lett.* 13, 4980–4988. doi:10.1021/nl403149u

Zhang, S. Y., Regulacio, M. D., and Han, M. Y. (2014). Self-assembly of colloidal one-dimensional nanocrystals. *Chem. Soc. Rev.* 43, 2301–2323. doi:10.1039/c3cs60397k

Zhang, Z., and Lin, M. (2014). High-yield preparation of vertically aligned gold nanorod arrays via a controlled evaporation-induced self-assembly method. *J. Mat. Chem. C* 2, 4545–4551. doi:10.1039/c4tc00325j

Zhu, Z., Meng, H., Liu, W., Liu, X., Gong, J., Qiu, X., et al. (2011). Superstructures and SERS properties of gold nanocrystals with different shapes. *Angew. Chem. Int. Ed.* 50, 1593–1596. doi:10.1002/anie.201005493